Commun. Comput. Phys.
doi: 10.4208/cicp.220115.071215a

Vol. **20**, No. 2, pp. 279-300
August 2016

Analysis of the Effect of Spatial Uncertainties on the Dynamic Behavior of Electrostatic Microactuators

Aravind Alwan[1] and Narayana R. Aluru[1,*]

[1] *Department of Mechanical Science and Engineering, Beckman Institute for Advanced Science and Technology, University of Illinois at Urbana-Champaign, 405 N. Mathews Avenue, Urbana, IL 61801, USA.*

Received 22 January 2015; Accepted (in revised version) 7 December 2015

Abstract. This paper examines the effect of spatial roughness on the dynamical behaviour of electrostatic microactuators. We develop a comprehensive physical model that comprises a nonlinear electrostatic actuation force as well as a squeeze-film damping term to accurately simulate the dynamical behavior of a cantilever beam actuator. Spatial roughness is modeled as a nonstationary stochastic process whose parameters can be estimated from profilometric measurements. We propagate the stochastic model through the physical system and examine the resulting uncertainty in the dynamical behavior that manifests as a variation in the quality factor of the device. We identify two distinct, yet coupled, modes of uncertainty propagation in the system, that result from the roughness causing variation in the electrostatic actuation force and the damping pressure, respectively. By artificially turning off each of these modes of propagation in sequence, we demonstrate that the variation in the damping pressure has a greater effect on the damping ratio than that arising from the electrostatic force. Comparison with similar simulations performed using a simplified mass-spring-damper model show that the coupling between these two mechanisms can be captured only when the physical model includes the primary nonlinear interactions along with a proper treatment of spatial variations. We also highlight the difference between nonstationary and stationary covariance formulations by showing that the stationary model is unable to properly capture the full range of variation as compared to its nonstationary counterpart.

PACS: 02.50.Ey, 02.70.Dh, 02.70.Uu, 46.15.-x, 47.61.Fg

Key words: Uncertainty quantification, microelectromechanical systems (MEMS), electrostatic actuation, squeeze-film damping, roughness, random process, damping ratio.

*Corresponding author. *Email addresses:* aalwan2@illinois.edu (A. Alwan), aluru@illinois.edu (N. R. Aluru)

1 Introduction

The accurate dynamic analysis of micromechanical actuators has been the subject of a lot of research and have led to the development of precise electromechanical resonators [1–4]. Due to the nature of the manufacturing process involved in their fabrication, microsystem designers have to account for several uncertainties in the form of variation in the properties of these devices [5, 6]. The study of these uncertainties is important for understanding their effect on the performance of a device as well as in modifying its design to make it robust towards these variations [7–9]. In this paper, we are concerned with the outcome of spatial variations in dimensional parameters on the dynamical behavior of microelectromechanical systems (MEMS). We focus on systems like oscillators and resonators that are driven using electrostatic actuation, since the electric field that is used for actuation in these systems, is particularly sensitive to spatial perturbations in the geometry of the device. Using stochastic models to establish a formal description of spatial uncertainties, we try to predict the resulting variation in the quality factor associated with these resonators, which is a relevant performance metric. The goal is to use a proper physical model in order to identify the dominant mode of uncertainty propagation in such devices and thereby understand the role that spatial variations play in them.

A simple electrostatic microactuator can be modeled as a pair of conducting electrodes, one of which is held fixed while the other is allowed to move. A potential difference applied between the two electrodes creates an electric field that results in an attractive electrostatic force. The movable electrode is either attached to a mechanical spring or is compliant enough to deform under the action of the applied force, while being anchored at one or more locations, and is responsible for converting the electrostatic force into a displacement [10–12]. In addition to the mechanical restoring force offered by the compliant structure, the motion of the movable electrode is also retarded by various damping phenomena. At meso- and micro-scales, the principle cause of damping is the surrounding medium, which is typically air. This can be suitably modeled using squeeze film damping theory, where the film of air that gets trapped between the electrodes, when the device oscillates at relatively high frequencies, causes a back-pressure that retards the motion of the system [13]. The magnitude of the electrostatic force is intimately linked with the nature of the electric field generated between the electrodes. As such, any spatial variation of the surfaces of these electrodes will lead to changes in the electric field and ultimately, the displacement as well. Spatial roughness also affects the damping force, since it modifies the flow of air in the squeeze-film region. This can affect the dynamic behavior of electrostatic oscillators operating at high frequencies and can be quantified by observing the variation in the quality factor, which is a measure of ratio of energy stored in an oscillator to the energy that is dissipated [14].

Surface variations in MEMS are usually modeled either using stochastic processes, where the roughness is specified in terms of a local covariance structure [6, 15], or using self-affine roughness models, where the roughness spectrum is assumed to have a power law scaling [16, 17]. The effect of spatial roughness on the dynamical behavior of

MEMS has been studied in the context of variation in the Casimir force acting on electromechanical switches [17,18], which modifies the static and dynamic behavior of these devices [19]. However, the spatial variations considered in these studies were restricted to those naturally present in gold thin film surfaces, where the amplitude of roughness can be controlled down to the order of a few nanometers. Consequently, they only considered the role of roughness on Casimir force, which becomes important at those scales. In a generic micromechanical system, the final surface texture could be the result of a number of processing steps involving multiple iterations of patterning, etching and deposition. As a result, we may expect to see spatial variations at larger length scales as well. Moreover, the physical models used in the aforementioned studies were restricted to 1-D approximations of the system, where perturbations in the damping force were not considered. In this work, we model spatial uncertainties using stochastic processes, whose parameters can be estimated from multiple sets of profilometric measurements of the surface height. This framework allows us to incorporate non-stationarity in the stochastic models, since this may have an effect on the resulting device behavior as well. We also use a more comprehensive physical model to capture the dynamics of the system so that we can understand the principal mode of uncertainty propagation.

The primary contribution of this paper is to demonstrate that the presence of micron-scale spatial variations translates into uncertainty in both the actuation force as well as the air damping. Due to the nonlinear, coupled nature of the interaction between these two, we show that it is important to consider a proper physical model in order to properly capture these variations. Using results obtained from numerical simulations, we argue that the quality factor of an electromechanical resonator is mainly affected by perturbations to the damping force, although the variation in actuation force does have a role to play as well. The goal of this work is to provide a framework for simulating such uncertainties and to guide the design of electrostatic actuators in order to make their performance robust towards the effect of these variations. The outline of the paper is as follows: Section 2 outlines the physical model used to describe electrostatic actuators. The stochastic process formulation used to represent spatial variations is covered in Section 3. The results of uncertainty propagation are then discussed in Section 4, where we examine the role of roughness on the different forces present in the system. The concluding remarks are presented in Section 5.

2 Physical model

We are interested in performing UQ for microelectromechanical actuators, which employ electrostatic force as the primary actuation mechanism. As shown in Fig. 1, these actuators can be modeled as a pair of electrodes, of which one is deformable while the other is held fixed at a small distance away. The region between the electrodes is considered to be a uniform dielectric material, usually air. A potential difference that is applied across the two electrodes sets up an electric field in the region between them. This results in

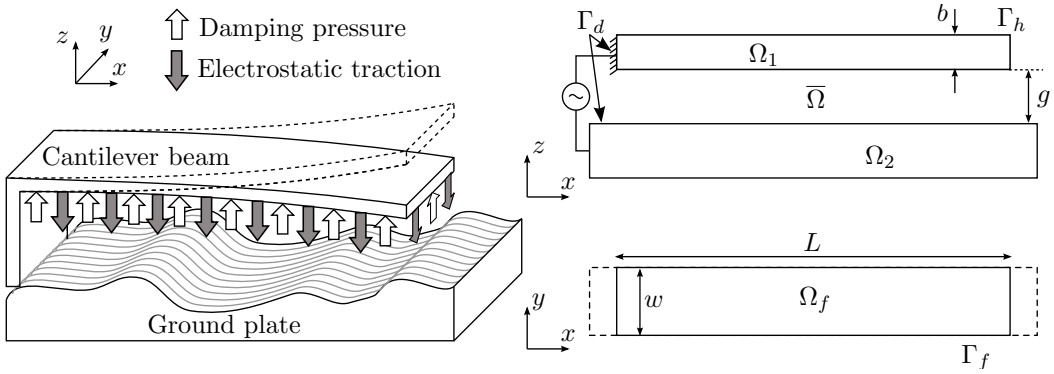

Figure 1: Schematic of the cantilever beam actuator showing the different forces acting on the movable beam (left) along with the domains used for mechanical and electrostatic analysis (top right) as well as fluidic analysis (bottom right) in the numerical model (right).

an attractive electrostatic force on the compliant electrode, causing it to deform. The air medium is also responsible for providing mechanical damping that retards the motion of the cantilever.

The actuator domain is modeled as shown on the right side of Fig. 1. The two electrodes are assumed to be perfect conductors and are represented in their initial undeformed configuration as Ω_1 and Ω_2, while $\overline{\Omega}$ refers to the dielectric region surrounding the electrodes. The top electrode is deformable and is anchored at its left end. Since the electrostatic traction as well as the damping pressure have a nonlinear dependence on the separation between the electrodes, we need to solve for the unknown state variables in a coupled manner to ensure a consistent solution. This is done by expressing the equations using a Lagrangian formulation, where the equations are expressed for the system in the deformed configuration and then mapped back to the undeformed configuration by means of the deformation gradient tensor, $\boldsymbol{F}$. We assume that the width, w, of the cantilever beam is large enough that a plane strain approximation can be used to reduce the elasticity equations to the x-z plane. Using a 2D geometrically nonlinear elastodynamics formulation [20], the displacement of the deformable electrode is given by,

$$\rho\ddot{\boldsymbol{u}} = \nabla\cdot(\boldsymbol{FS}) \quad \text{in } \Omega_1, \tag{2.1}$$

$$\boldsymbol{u} = \boldsymbol{0} \quad \text{on } \Gamma_d, \tag{2.2}$$

$$\boldsymbol{P}\cdot\boldsymbol{N} = \boldsymbol{H}_f + \boldsymbol{H}_e \quad \text{on } \Gamma_h, \tag{2.3}$$

$$\boldsymbol{u}|_{t=0} = \dot{\boldsymbol{u}}|_{t=0} = 0 \quad \text{in } \Omega_1, \tag{2.4}$$

where ρ is the mass density of the cantilever beam, $\boldsymbol{u}$, $\dot{\boldsymbol{u}}$ and $\ddot{\boldsymbol{u}}$ are the vector fields corresponding to displacement, velocity and acceleration, respectively, $\boldsymbol{F} = \boldsymbol{I} + \nabla\boldsymbol{u}$, $\boldsymbol{I}$ being the identity tensor, Γ_d is the anchored portion of the electrode boundary corresponding to a Dirichlet boundary condition, $\boldsymbol{P}$ is the first Piola-Kirchhoff stress tensor and $\boldsymbol{N}$ is the outward normal vector at every part of the boundary in the reference configuration. The

terms, $\boldsymbol{H_f}$ and $\boldsymbol{H_e}$, are the boundary traction vectors corresponding to electrostatic and damping traction respectively, that act on the free surfaces of the movable electrode, Γ_h. $\boldsymbol{S}$ in Eq. (2.1) is the second Piola-Kirchhoff stress tensor that can be expressed in terms of a constitutive relationship involving the material tensor, $\boldsymbol{C}$, and Green-Lagrangian strain tensor, $\boldsymbol{E_s}$, as [21],

$$\boldsymbol{S}=\boldsymbol{C}\boldsymbol{E_s},\quad \boldsymbol{E_s}=\frac{1}{2}\left[\boldsymbol{F}^T\boldsymbol{F}-\boldsymbol{I}\right]. \tag{2.5}$$

We see that the driving force for the mechanical displacement is the electrostatic traction, which can be obtained by solving for the electrostatic potential. Since the electrodes are assumed to be metallic, the electric field within them is zero and so, it is sufficient to solve for the potential field in the dielectric region surrounding the electrodes. This can be written in terms of the Laplace equation, with a Dirichlet boundary condition on the boundaries of the electrodes, as,

$$\nabla\cdot\left(J\boldsymbol{F}^{-1}\boldsymbol{F}^{-T}\nabla\psi\right)=0\quad \text{in } \overline{\Omega}, \tag{2.6}$$

$$\psi=\psi_0\quad \text{on } \Gamma_d, \tag{2.7}$$

where $J=det\boldsymbol{F}$ is the Jacobian of the deformation gradient and ψ_0 is the prescribed potential applied on the boundaries of the electrodes. The electrostatic potential that is obtained by solving Eq. (2.6) is coupled back to the mechanical displacement by way of the electrostatic traction term, $\boldsymbol{H_e}$, which is given by,

$$\boldsymbol{H_e}=J\left|\boldsymbol{F}^{-T}\boldsymbol{N}\right|\boldsymbol{f}_{es}, \tag{2.8}$$

where $\boldsymbol{f}_{es}$ is the electrostatic traction acting on the movable electrode in the deformed configuration. This traction depends on the normal electric field at the interface between the electrode and the dielectric, E_n, and the surface charge density, $\sigma_s=\epsilon E_n$, where E_n is the normal component of the electric field, $\boldsymbol{E}=-\nabla\psi$, along the unit normal vector in the deformed configuration, $\boldsymbol{n}$. The complete expression for the electrostatic traction is given by, $\boldsymbol{f}_{es}=[{\sigma_s}^2/(2\epsilon)]\boldsymbol{n}$, where ϵ is the dielectric permittivity of the surrounding medium.

In practice, we do not solve Eq. (2.6) directly, since it is defined over $\overline{\Omega}$, which is infinitely large. Instead we transform this equation using boundary integral formulation [22, 23] into a set of integral equations defined on the boundaries of the electrodes. The boundary integral formulation is an efficient way of solving the Laplace equation for exterior-domain problems such as this one. Additional details about this procedure are given in [12, 24].

The ambient air pressure acts on all sides of the cantilever, with the pressure acting on the short edge and the top edge not varying significantly from the ambient air pressure, P_a. However, due to the motion of cantilever, the air film between the cantilever and the ground plate gets squeezed, resulting in a back-pressure that damps the motion of the beam. Since the gap of the cantilever is very small compared to its width and length, the pressure is assumed to be uniform in the z-direction. The fluid damping problem can be

solved in the domain obtained by taking the projection of the cantilever beam on the x-y plane. The fluid pressure in this domain is governed by the isothermal Reynolds squeeze film damping (RSFD) equation [4, 25],

$$\frac{\partial}{\partial x}\left[(1+6K_n)h^3P_f\frac{\partial P_f}{\partial x}\left(1+\frac{\partial u_x}{\partial x}\right)^{-1}\right]\left(1+\frac{\partial u_x}{\partial x}\right)^{-1} + \frac{\partial}{\partial y}\left[(1+6K_n)h^3P_f\frac{\partial P_f}{\partial y}\right] = 12\eta\frac{\partial\left(hP_f\right)}{\partial t} \quad \text{in } \Omega_f, \tag{2.9}$$

$$P_f = P_a \quad \text{on } \Gamma_f, \tag{2.10}$$

where K_n is the non-dimensional Knudsen number, h is the point-wise separation or gap height between the cantilever and the ground plate, u_x is the x-component of the displacement vector, $\boldsymbol{u}$, and η is the viscosity of the fluid medium. The height, h, is obtained from the mechanical displacement of the beam as $h(x) = g + u_z(x)$, where g is the gap between the electrodes in the undeformed configuration. The $\left(1+\frac{\partial u_x}{\partial x}\right)^{-1}$ factor that appears in the first term on the left hand side of Eq. (2.9), is due to the Lagrangian formulation, where a mapping is performed in order to transform the projected fluid domain to its counterpart, Ω_f, in the undeformed configuration. We assume that the pressure fluctuations die out at the boundary, Γ_f, of the fluid domain. This is represented as a Dirichlet boundary condition in Eq. (2.10). The damping pressure on the mechanical structure along the bottom edge can be obtained by integrating the fluid pressure across the y direction to get the traction per unit width as,

$$\boldsymbol{H}_f = -\frac{1}{w}\left(\int_0^w \left(P_f - P_a\right) dy\right) J\boldsymbol{F}^{-T}\boldsymbol{N}. \tag{2.11}$$

3 Modeling spatially varying random fields

In this section, we first introduce the concept of a stochastic process, which is a collection of random variables that are indexed by some parameter. A spatially varying uncertainty can be modeled in terms of a random field, which in turn is a generalization of a stochastic process, where the underlying parameter that is used to index the collection of random variables is a spatial location. In this work, we use a Gaussian process (GP) framework to model spatially varying random fields. A Gaussian process, f, is a generalization of the multivariate normal distribution [26], where the value of the process at each point in a domain is a random variable and the random spatial variations are described as fluctuations about a mean function, $M(X)$. The fluctuations are assumed to be spatially correlated and this dependence is parameterized in terms of a covariance function, $C(X, X')$, which quantifies the covariance between the values of the Gaussian process at two points, X and X', in the domain of the stochastic process. It follows that

for a finite set of points in the domain, $\boldsymbol{X}=\{X_j;j=1,2,\cdots,n\}$, the corresponding set of random variables at these points, $\boldsymbol{d}$, is distributed according to a multivariate Gaussian distribution as,

$$\boldsymbol{d}\sim\frac{1}{(2\pi)^{n/2}|\boldsymbol{\Sigma}|^{1/2}}\exp\left[-\frac{1}{2}(\boldsymbol{X}-\boldsymbol{\mu})^T\boldsymbol{\Sigma}^{-1}(\boldsymbol{X}-\boldsymbol{\mu})\right], \tag{3.1}$$

where $\boldsymbol{\mu}$ is the mean vector, whose components are given by $\mu_j=\mathbb{E}[f(X_j)]=M(X_j)$, and Σ is the covariance matrix given by $\Sigma_{ij}=\text{Cov}(f(X_i),f(X_j))=C(X_i,X_j)$ for $i,j=1,2,\cdots,n$ [27].

In order to estimate the Gaussian process stochastic model, we first choose a form for the mean and covariance functions such that the stochastic model can be parameterized in terms of a set of unknown hyperparameters. Thus, the task of estimating the stochastic model reduces to one of fitting the hyperparameters to the given dataset. The mean function can be parameterized by choosing a basis representation that can adequately capture the average trend in the data. In this work, we use a polynomial representation for the mean function in order to demonstrate the process, although other basis sets may be more appropriate depending on the application.

For the covariance function, we usually choose an appropriate family of covariance functions as the parametric form and fit the hyperparameters to the data. Popular choices for the parameterization are the exponential and Gaussian families of covariance functions. This works well when the covariance function is known to be stationary, where the covariance between the values at two points, X and X', only depends on the distance, $\|X-X'\|$, between them. To handle nonstationary covariance functions, we employ a coordinate transformation to map the arguments, X and X', of the covariance function, to new locations, x and x', such that $C(x,x')$ is an equivalent stationary covariance function, which can be parameterized as above [28]. We use an additive model for the transformation, in which the displaced co-ordinate is expressed as, $x(X)=X+u(X)$, where $u(X)$ is a fictitious displacement function that encapsulates the nonstationarity in the covariance function. Putting all of the above together, we get the following form for the stochastic model:

$$\begin{aligned}
f|M,C&\sim GP(M,C),\\
M:X,a,b,c&\mapsto aX^2+bX+c,\\
C:x,x',\nu,\phi,\theta&\mapsto Matérn\left(x,x',\nu,\phi,\theta\right),\\
x:X,u&\mapsto X+u(X),\\
u:X,a_u,b_u,c_u,d_u&\mapsto a_uX^3+b_uX^2+c_uX+d_u,\\
\boldsymbol{d}|M,C&\sim\mathcal{N}(M(\boldsymbol{X}),C(x(\boldsymbol{X}),x(\boldsymbol{X}))),
\end{aligned} \tag{3.2}$$

where we have used a quadratic polynomial to represent the mean function and a cubic polynomial to represent $u(X)$. We use the Matérn family of covariance functions to parameterize $C(x,x')$, since this is a more general class of covariance functions in which the exponential and Gaussian families are special cases. The Matérn covariance function is

given by [27],

$$Matérn\left(X,X',\nu,\phi,\theta\right)=\phi^2\frac{1}{\Gamma(\nu)2^{\nu-1}}\left(\sqrt{2\nu}\frac{\|X-X'\|}{\theta}\right)^{\nu}K_{\nu}\left(\sqrt{2\nu}\frac{\|X-X'\|}{\theta}\right), \tag{3.3}$$

where Γ is the Gamma function, while K_ν is the modified Bessel function of the second kind. ν, ϕ and θ are parameters that characterize the covariance function. ν represents the differentiability of the resulting random process, while ϕ^2 is the amplitude of the covariance function and is proportional to the point-wise variance of the random process. θ is a scaling parameter that varies with the scale of the domain. In the above formulation, the terms, a, b, c, a_u, b_u, c_u, d_u, ν, ϕ and θ are unknown parameters, which shall be later determined as a part of the estimation procedure.

It is important to note that the choice of basis functions and the form of parameterization used above is only meant to serve an illustrative purpose. The actual choice of the formulation may be varied based on the characteristics of the stochastic data that is available so that a good fit is obtained. Depending on the choice of parameterization, we obtain a variety of models that can be fit to the available data. A rigorous model selection procedure may be adopted to choose the model that best fits the uncertainty in the data [27]. Having chosen a representation for the stochastic process, we can identify unknown parameters in the model that need to be determined using the measured data. The process of estimating the random process involves choosing an appropriate set of values for the unknown parameters in Eq. (3.2) for a given set of values for $\boldsymbol{d}$, so that the resulting random process closely matches the actual, unknown process from which the dataset is derived. A thorough discussion of this procedure may be found in [29]. We use Bayesian inference to perform the model estimation, in which we first assign prior probability density functions (PDF) to the unknown parameters and then compute the posterior PDFs under the influence of the data. This algorithm is implemented numerically using the PyMC software library [30], that uses the Markov Chain Monte Carlo (MCMC) method to estimate the stochastic process and draw samples from it that are consistent with the randomness in the data. These samples of the random surface may be directly used to modulate the finite element mesh to incorporate spatial uncertainties in the numerical model of the device that we are interested in.

4 Results

In this section, we examine the effect of spatial variations on the dynamical behavior of electrostatic actuators. We choose the example of a cantilever beam actuator, since it is the simplest representation of the system that we are interested in and it serves to demonstrate the physics of the problem. The dimensions of our cantilever are $l=100\,\mu$m, $b=1\,\mu$m, and $w=10\,\mu$m in an environment of air at 1atm pressure and a temperature of 300K. The cantilever beam is suspended above a substrate at a distance of $2\,\mu$m and a potential difference is applied between the two to generate electrostatic force.

We assume that the ground plate surface is not uniform, but rather it has spatial variations described by the stochastic process mentioned in the previous section. Our first task is to generate datasets from a known random process and then estimate the stochastic variation from the data. The estimated process can then be propagated through the physical model along with the actual process in order to demonstrate the effectiveness of estimating spatial uncertainties in this manner. Following the same procedure described in the previous section, we generate data from a known random process that is defined in the domain $[-10,110]\mu$m, assuming that the ground plate extends 10μm on either side of the cantilever beam. We pick a linear mean function, $M(X)=(0.05+0.005X)\mu$m, and a Matérn covariance function with the parameters: $\phi=0.1\mu$m, $\nu=2$ and $\theta=20\mu$m. To simplify notation, we introduce a normalized spatial coordinate $X_n=(X+10)/120$, such that $X_n\in[0,1]$, and re-define the mean function in terms of X_n as $M(X_n)=0.6X_n$. It is easily seen that the spatial roughness profile that we have chosen, causes the top surface of the ground plate to tilt upwards, reducing the gap at the right end of the cantilever to about 70% of its original value of 2μm on average. The choice of the mean function profile is arbitrary, but the parameters that contribute to the spatial roughness profile are based on physically measured roughness profiles of photoresist films [31].

Nonstationarity is introduced using a virtual displacement function and we choose two cases to demonstrate two different forms of nonstationarity. We denote $u(X_n)=X_n(1-X_n)(2-X_n)$ as Case I. This corresponds to a virtual displacement that is directed towards the right side or the free end of the actuator, since it is positive in the given domain. Case II is the opposite with $u(X_n)=-X_n(1-X_n^2)$, which corresponds to a displacement that is directed towards the left side or the anchored end. Using the datasets generated for Case I and Case II, we estimate the corresponding stochastic processes. We use a nonstationary formulation that is very similar to Eq. (3.2), except for a slight modification in the form of the displacement function, to make its value go to zero at either end of the domain. It is seen that this form of the displacement function differs from that in Eq. (3.2) only by a linear term and it can be shown that the resulting covariance function is identical under this modification [29,32]. The final formulation is given by:

$$\begin{aligned}
f|M,C &\sim GP(M,C),\\
M:X_n,a,b,c &\mapsto aX_n^2+bX_n+c,\\
X_n:X &\mapsto (X+10)/120,\\
C:x,x',\nu,\phi,\theta &\mapsto Matérn\left(x,x',\nu,\phi,\theta\right),\\
x:X_n,u &\mapsto -10+120(X_n+u(X_n)),\\
u:X_n,a_u,b_u &\mapsto a_uX_n^3+b_uX_n^2-(a_u+b_u)X_n,\\
\boldsymbol{d}|M,C &\sim \mathcal{N}(M(\boldsymbol{X}),C(x(\boldsymbol{X}),x(\boldsymbol{X}))).
\end{aligned} \tag{4.1}$$

We also assign prior PDFs to the unknown parameters in order to obtain their poste-

rior estimates using the generated datasets. The prior PDFs are as follows,

$$\begin{aligned} a,b,c &\sim Uniform[-1,1], \\ \nu &\sim Exponential(10), \\ \phi &\sim Exponential(20), \\ \theta &\sim Exponential(0.1), \\ a_u,b_u &\sim Uniform[-5,5], \end{aligned} \tag{4.2}$$

where we have chosen prior PDFs such that their range is approximately of the same order of magnitude as the values used to generate the data. Using these priors and the formulation given above, we estimate a nonstationary stochastic process model corresponding to the given data. We also compare this with another estimated model, where the displacement function is set to zero so that the resulting covariance function is stationary. We shall see the effect of propagating these two stochastic models through the device and demonstrate the need for proper nonstationary modeling when dealing with spatial uncertainties.

4.1 Variation of damping ratio

It can be immediately seen that as a result of the spatial variations, the gap between the cantilever beam and the ground plate is not constant, even when there is no deformation in the cantilever beam. The spatial roughness directly affects the damping pressure, since it is coupled into the RSFD equation by way of the gap height term, $h(x)$, as seen in Eq. (2.9). In addition to this effect, the roughness affects the magnitude of the electrostatic force acting on the beam, which in turn changes the amplitude of beam displacement. In contrast to the variation in damping pressure, the electrostatic force variation has only an indirect effect on the damping ratio by way of changing the amplitude of displacement, which has a corresponding effect on the damping pressure due to the nonlinear nature of the RSFD equation (Eq. (2.9)). Since there are two routes of uncertainty propagation, it would be interesting to see which one is more dominant and thus is more responsible for the variation in the damping characteristics. We take the realizations generated from the actual model for both Case I and Case II and compute the change in damping ratio in the presence of these variations. Fig. 2 shows the corresponding PDFs of the damping ratio.

Narrowing our focus to the blue lines that correspond to the full system, we see that there is a significant difference between the PDFs for Case I and Case II, with the latter showing a narrower range of variation. These two cases correspond to the two different forms of the nonstationary covariance function, where the region near the cantilever tip is relatively smooth for Case I whereas Case II is smoother in the region close to the anchor. From Eq. (2.9), we can infer that the effect of squeeze film damping will be inversely proportional to the gap between the cantilever and the ground plate. If the spatial profile of the surface varies rapidly about its mean value, then we can expect that the net effect on the damping pressure from the positive and negative contributions will approximately

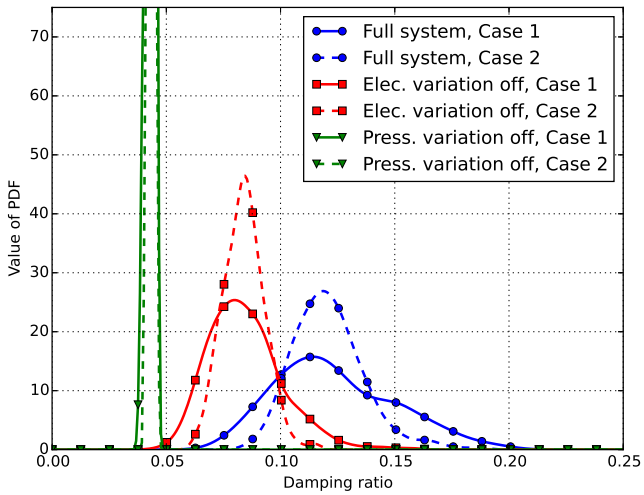

Figure 2: Variation of damping ratio due to spatial realizations generated from the actual stochastic model for Case I and II under three different physical conditions.

even out. However, in the smoother regions, where the spatial profile is more correlated, we expect to see a marked shift in the damping pressure. We know that the squeeze-film pressure profile is zero near the anchor and increases as we go towards the cantilever tip since it is proportional to the beam displacement. This means that fluctuations in the pressure near the tip have a greater effect on the total damping force than those near the anchor. This explains why we observe a greater range of variation in the damping ratio for Case I, since the smoother regions, which cause a greater shift in the damping pressure, are closer to the cantilever tip, where the magnitude of damping pressure is higher. We can also argue that since the cantilever is more compliant near its tip, the fluctuations in the damping force there have a greater effect on the system than fluctuations of the same magnitude near the anchor. This serves as another reason to explain why the range of variation is much higher for Case I.

4.2 Variation of potential energy

As mentioned earlier, the effect of spatial variation not only propagates into the damping pressure, but it also modifies the electrostatic force. Just like the damping pressure, the electrostatic traction is also inversely proportional to the gap between the electrodes. Hence, we expect to see a similar trend in the variation of electrostatic force when we compare Case I to Case II. It is interesting to note that the electrostatic and damping forces are linked to one another. Since both forces depend on the displacement of the cantilever, as the magnitude of one changes, it affects the displacement and thereby changes the magnitude of the other. Hence, it is impossible to completely divorce the effect of the two mechanisms of uncertainty propagation as far as the damping ratio is concerned.

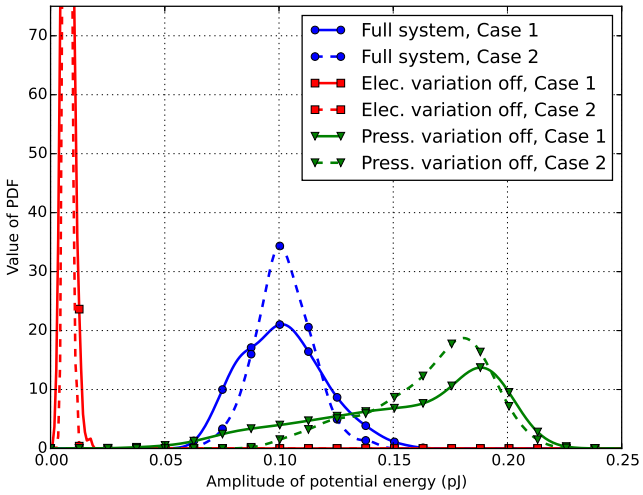

Figure 3: Variation of amplitude of potential energy due to spatial realizations generated from the actual stochastic model for Case I and II under three different physical conditions.

In order to gain more physical insight into the underlying mechanism, we look at the variation of the potential energy of the system. This is a relevant parameter because for a periodically oscillating system, the damping ratio is calculated as the ratio of the total energy dissipated in a single oscillation period to the amplitude of the potential energy. The potential energy of the system is roughly proportional to the electrostatic driving force, whereas the energy dissipated is the work done in overcoming the damping force. Therefore we shall use the potential energy amplitude as a means to separate out the roles of two uncertainty propagation mechanisms in causing the variation in the damping ratio. The PDFs of the amplitude of potential energy for the full system are shown as blue lines in Fig. 3. Again we see that the PDFs for Case I and Case II have some differences, but the difference in the range of variation is not as much as it was for the damping ratio in Fig. 2. This is expected because the variation in the damping ratio is the result of uncertainty in both the electrostatic force as well as the damping pressure.

4.3 Turning off electrostatic force variation

Having identified two different mechanisms of uncertainty propagation, the easiest way to compare the effect of the two is to examine them in isolation. As explained earlier, in the real device, these two are inextricably linked. However, in the numerical simulations, we have the luxury of artificially turning off one or both routes of uncertainty propagation. We first take the case of electrostatic force. From Section 2, we know that the electrostatic force is obtained by solving Eq. (2.6) in the air domain. The effect of spatial variations is introduced by modulating the domain boundary mesh to match the realiza-

tions generated from the stochastic model. By solving Eq. (2.6) on the original domain without applying the spatial variations, we can effectively decouple the spatial variations from the electrostatic force computation.

The PDFs of the damping ratio and the potential energy amplitude, computed without the effect of spatial roughness on electrostatic force, are shown as red lines in Fig. 2 and Fig. 3 respectively. We can immediately see that when the electrostatic force variation is turned off, both the mean and the variance of the potential energy amplitude are decreased. The potential energy is related to the square of the displacement amplitude, as is the energy dissipated per cycle, if nonlinear effects on damping pressure are not considered. Hence, for a linear system, the drop in potential energy is compensated by a corresponding drop in the energy dissipated and the net result is that the damping ratio remains roughly the same. However, since the RSFD equation has a nonlinear dependence on the gap height (and consequently, the displacement amplitude), we hypothesize that the drop in the damping pressure will be slightly more and hence, we expect to observe a drop in the net damping ratio. This is borne out in Fig. 2, where we see that the red lines are shifted a good deal to the left of the blue ones, showing that when the electrostatic variation route is turned off, the mean value of the damping ratio is almost half that of the full system. However, we still see a fair bit of variation in the damping ratio, evidently due to the direct fluctuations in damping pressure which are still present in the system.

4.4 Turning off damping pressure variation

We now consider the opposite situation, where the spatial variations are considered during the computation of the electrostatic force, but not while solving the RSFD equation. In other words, we still compute the gap height as $h(x)=g+u_z(x)$, but assume that g is equal to the nominal gap height in the undeformed configuration and does not vary with the roughness in the ground plate. This allows us to decouple the spatial variations from the damping pressure calculations. However, it must be noted that since the roughness does modulate the electrostatic force, the uncertainty will ultimately get coupled into the damping pressure as well through the displacement term, $u_z(x)$.

We compute the PDFs of damping ratio and potential energy amplitude, which are shown as green lines in Fig. 2 and Fig. 3 respectively. We observe that in the absence of spatial variations directly modulating the damping pressure, the damping ratio reduces to almost a third of its original value corresponding to the full system. The amplitude of potential energy, on the other hand, is seen to be higher than that for the full system. However, the increase in the potential energy is less than the proportionate decrease in the damping ratio, indicating that it cannot be the sole reason for this change. Moreover, as seen in the previous section, due to a coupling of the displacement amplitude into the damping pressure calculations, an increase in the potential energy amplitude should actually cause an increase in the energy dissipated per cycle. Since the damping ratio is seen to decrease, despite this coupling, we conclude that the decoupling of pressure vari-

ations from the damping pressure calculation has a much greater effect on the damping ratio than due to the coupling through the electrostatic force. This means that the pressure damping route is the dominant mechanism for uncertainty propagation as far as the damping ratio is concerned.

4.5 Comparison with a 1D mass-spring-damper model

To further understand the role of nonlinear coupling in uncertainty propagation, we consider a simplified physical model for the system, where we simulate the dynamic behavior using a mass-spring-damper (MSD) model. The mass and spring constant used in the model are obtained by calculating the effective values corresponding to the first mode of a vibrating cantilever beam. The damping coefficient is obtained by modeling the squeeze-film damping for a pair of flat plates moving towards each other. The electrostatic force corresponds to that acting on the electrodes of a parallel plate capacitor, where the separation between the electrodes is equal to the sum of the undeformed gap height and the amplitude of displacement of the first mode of the cantilever beam. The final expression for the motion of the MSD system is given by,

$$m\ddot{s}+c\dot{s}+ks=\frac{\epsilon wLV^2}{2(g-s)^2}, \tag{4.3}$$

where m, c and k are the effective mass, damping coefficient and stiffness, respectively, of the first transverse vibration mode of the cantilever beam and s is the modal displacement amplitude taken to be positive in the negative z-direction. First of all, we note that the nominal gap-height, g, figures in the computation of the electrostatic force as well as the damping coefficient. This is similar to the situation in the full numerical model, except that nonlinear variation of damping as well as spatial variations of the ground plate are ignored. In order to perform uncertainty propagation, we compute the average gap height over the spatial domain for each realization sampled from the stochastic model and apply that variation to the value of g.

The damping ratio and amplitude of potential energy are computed in the same way as for the numerical model, and the variation in these quantities are shown in Fig. 4 and Fig. 5 respectively. As in the case of the full numerical model, we compare the results with simulations where uncertainty propagation through either the electrostatic force or the damping coefficient is turned off. Since the MSD model is a drastic simplification of the physics in the full numerical model, we may at most expect to have a qualitative match with the results in Fig. 2 and Fig. 3. We observe that for the MSD model, the variation in the damping ratio is solely caused by the change in the value of c and that when the damping pressure variation is turned off, all the uncertainty in the damping ratio disappears. On the other hand, turning off the variation in the electrostatic force seems to have only a marginal effect on the damping. The plots for the potential energy amplitude all follow the same general trend as that seen in Fig. 3. Despite this qualitative match in the amplitude of potential energy, the simplified model is quite inaccurate in predicting

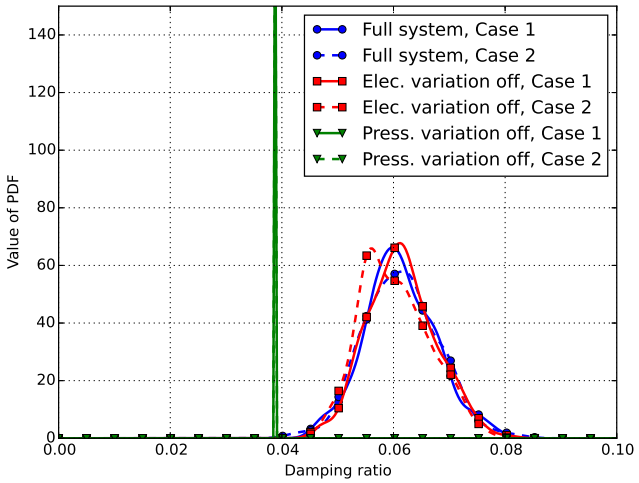

Figure 4: Damping ratio for the MSD model.

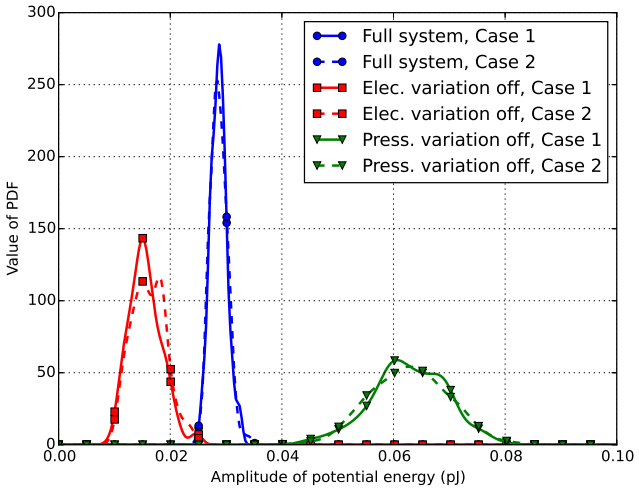

Figure 5: Amplitude of potential energy for the MSD model.

the variation in the damping ratio, even in terms of capturing the general trend. Moreover, we see that the estimated PDFs for Case I and Case II have almost no difference, showing that the MSD model is insensitive to the nonstationarity in the stochastic model. This shows the importance of properly accounting for spatial variations when performing numerical simulations so that the resulting predictions are more accurate. Fig. 6 and Fig. 7 summarize the damping ratio and potential energy amplitude results for Case I, by comparing the PDFs estimated using the full physical model presented in Section 2 with those obtained using the MSD approximation.

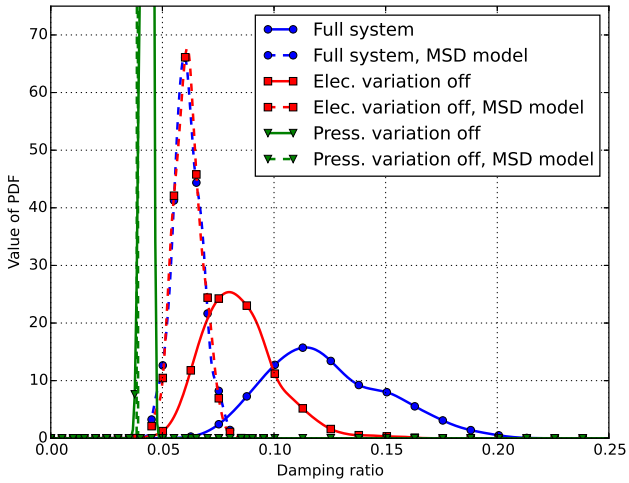

Figure 6: Damping ratio for Case I, estimated using the full physical model compared with that using the MSD model.

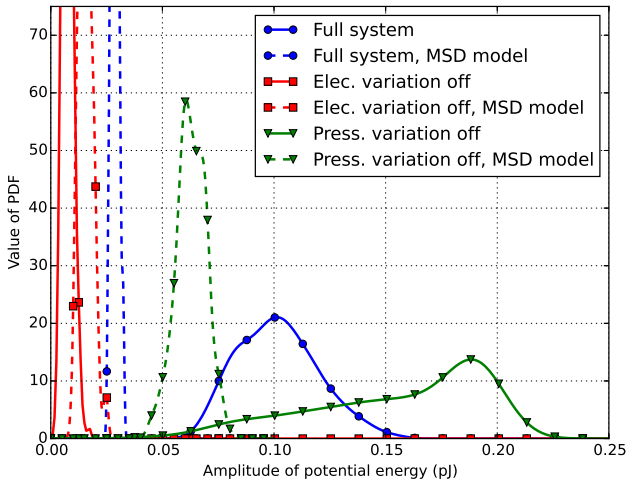

Figure 7: Amplitude of potential energy for Case I, estimated using the full physical model compared with that using the MSD model.

4.6 Importance of nonstationarity during stochastic modeling

In this section, we examine the importance of nonstationary stochastic modeling in the context of dynamic behavior. We gather the results predicted by the estimated stochastic models with nonstationary and stationary covariance functions and contrast them with results predicted by the actual model. The resulting PDFs are plotted in Figs. 8-13 for both damping ratio and amplitude of potential energy and for cases with and without

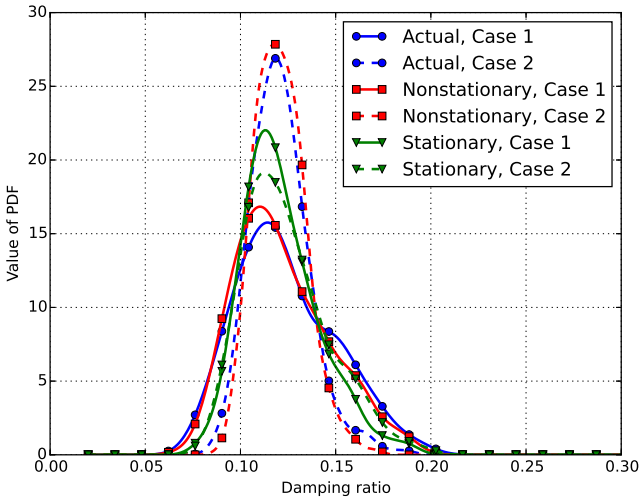

Figure 8: Damping ratio for the full system.

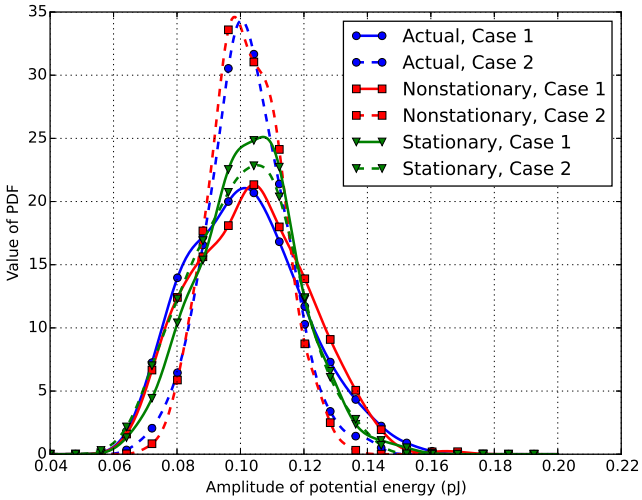

Figure 9: Amplitude of potential energy for the full system.

the variation in electrostatic force and damping pressure. In all the figures, we see that the results from the nonstationary model (red lines) show a close match with those from the actual model (blue lines), clearly distinguishing between Case I and Case II, the two types of nonstationarity that are considered. The stationary model (green lines) is unable to capture the spatial variation properly and hence, unable to distinguish between the two cases. Consequently, the corresponding results only capture an average sense of the variation seen in the two cases.

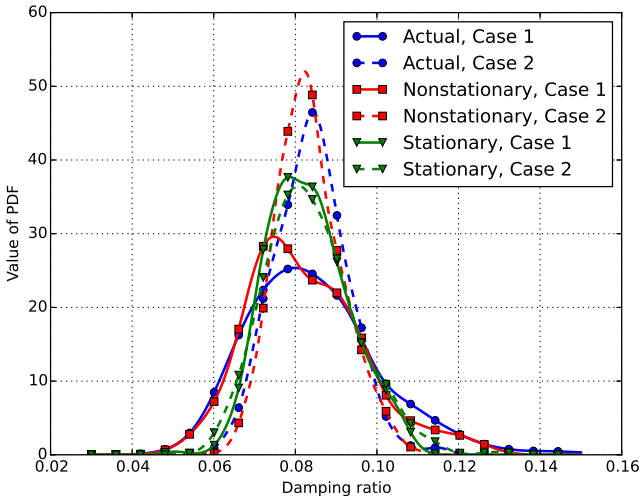

Figure 10: Damping ratio for the system with electrostatic force variation turned off.

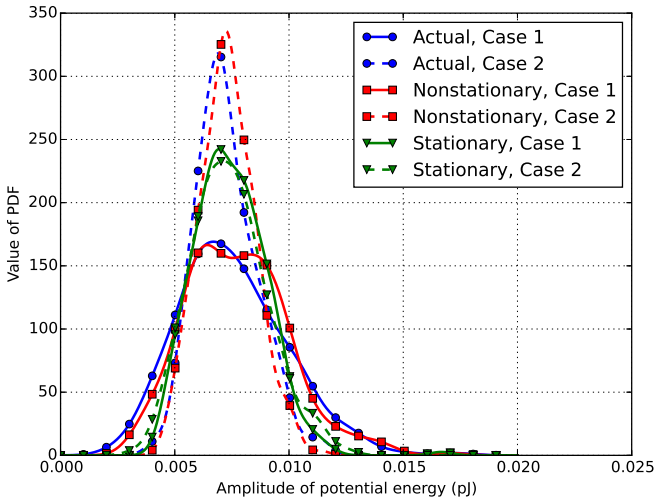

Figure 11: Amplitude of potential energy for the system with electrostatic force variation turned off.

5 Conclusions

The analysis of the dynamic behavior of microactuators presents a unique challenge due to the highly-coupled multiphysics interactions that are involved. These devices find applications in high-precision resonators and hence, they are particularly sensitive to small deviations from the nominal design. Since, random variations are an inevitable consequence of the nature of the microfabrication process, a proper uncertainty quantification

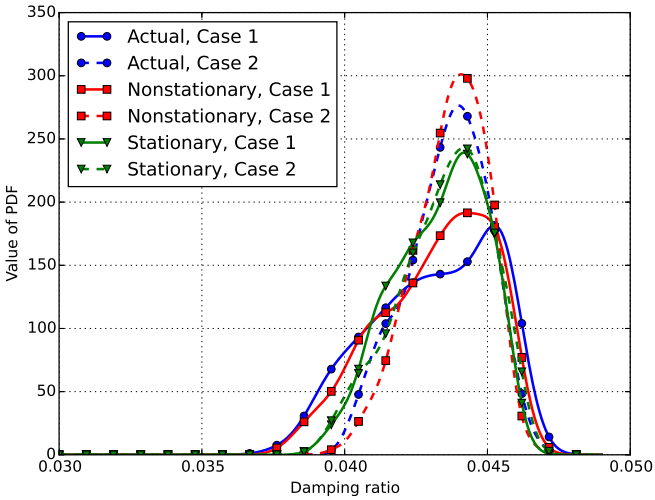

Figure 12: Damping ratio for the system with pressure variation turned off.

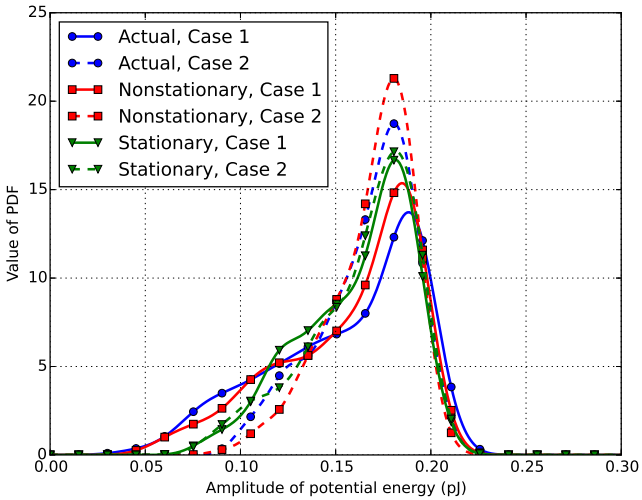

Figure 13: Amplitude of potential energy for the system with pressure variation turned off.

(UQ) framework is needed in order to successfully manufacture devices that meet performance specifications on a large scale. In this context, we model the effect of spatial variations on electrostatic microactuators and examine the propagation of uncertainty in the dynamical behavior of these devices.

Modeling spatial roughness as a stochastic process, we describe a framework to estimate stochastic models for the variation from sets of profilometric measurements. We use simulated data sampled from an assumed stochastic model and fit unknown parameters

in stationary and nonstationary covariance function formulations using Bayesian inference. Propagation of these uncertainties through the physical model shows that there is a significant variation in the damping ratio, which is a measure of the dynamic characteristics of the actuator. We postulate two different routes for uncertainty propagation involving variation in the electrostatic traction and the damping pressure terms, respectively. In order to identify the dominant cause for uncertainty, we artificially tweak the physical model by alternatively turning off each of these two routes.

The results obtained from each of these simulations show that the variation in damping pressure has a greater impact on the uncertainty in the damping ratio, while the electrostatic force variation is less significant. We contrast these simulations with similar ones performed using a simplified physical model where spatial variations are completely ignored. We see that although there is a similar trend in the damping ratio variation, the secondary coupling effects are completely absent. In particular, we see that the electrostatic force has almost no role to play in uncertainty propagation, which is a marked difference from the full physical model, where it does play an important role.

Due to inclusion of nonstationarity in the covariance function, we are able to compare the importance of this aspect of stochastic model generation. We see that the nonstationary covariance models compare well with the actual models used to generate data, whereas a stationary covariance assumption does not capture the variation well. In particular, we see that data corresponding to two different nonstationary covariance cases shows a marked difference in the predicted damping ratio. However, the stationary modeling approach only captures the average trend and fails to distinguish between these two cases. This is a uniform trend seen across all the simulation cases, showing that proper stochastic modeling is essential towards obtaining accurate predictions of variation in device performance.

Acknowledgments

This work is supported by the National Science Foundation under grant number 1420882. The authors gratefully acknowledge the use of the parallel computing resource provided by the Computational Science and Engineering (CSE) Program at the University of Illinois. The CSE computing resource, provided as part of the Taub cluster, is devoted to high performance computing in engineering and science.

References

[1] S. K. De and N. Aluru, "Full-Lagrangian schemes for dynamic analysis of electrostatic MEMS," *J. Microelectromech. Syst.*, vol. 13, no. 5, pp. 737–758, 2004.

[2] F. Shi, P. Ramesh, and S. Mukherjee, "Dynamic analysis of micro-electro-mechanical systems," *Int. J. Numer. Meth. Eng.*, vol. 39, no. 24, pp. 4119–4139, 1996.

[3] A. H. Nayfeh, M. I. Younis, and E. M. Abdel-Rahman, "Dynamic pull-in phenomenon in MEMS resonators," *Nonlinear Dynam.*, vol. 48, no. 1-2, pp. 153–163, 2007.

[4] S. K. De and N. Aluru, "Coupling of hierarchical fluid models with electrostatic and mechanical models for the dynamic analysis of MEMS," *J. Micromech. Microeng.*, vol. 16, no. 8, p. 1705, 2006.
[5] D. Xiu and G. Karniadakis, "Modeling uncertainty in flow simulations via generalized polynomial chaos," *J. Comput. Phys.*, vol. 187, pp. 137–167, May 2003.
[6] N. Agarwal and N. R. Aluru, "Stochastic analysis of electrostatic MEMS subjected to parameter variations," *J. Microelectromech. Syst.*, vol. 18, pp. 1454–1468, Dec. 2009.
[7] J. Han and B. Kwak, "Robust optimal design of a vibratory microgyroscope considering fabrication errors," *J. Micromech. Microeng.*, vol. 11, no. 6, p. 662, 2001.
[8] J. Wittwer, M. Baker, and L. Howell, "Robust design and model validation of nonlinear compliant micromechanisms," *J. Microelectromech. Syst.*, vol. 15, no. 1, pp. 33–41, 2006.
[9] A. Martowicz and T. Uhl, "Reliability-and performance-based robust design optimization of MEMS structures considering technological uncertainties," *Mech. Syst. Signal Pr.*, vol. 32, pp. 44–58, 2012.
[10] S. Senturia, N. Aluru, and J. White, "Simulating the behavior of MEMS devices: computational methods and needs," *IEEE Comput. Sci. Eng.*, vol. 4, pp. 30 –43, Jan.-Mar. 1997.
[11] N. Aluru and J. White, "An efficient numerical technique for electromechanical simulation of complicated microelectromechanical structures," *Sensor. Actuat. A-Phys.*, vol. 58, no. 1, pp. 1–11, 1997.
[12] G. Li and N. Aluru, "Efficient mixed-domain analysis of electrostatic MEMS," *IEEE T. Comput. Aid. D.*, vol. 22, pp. 1228 – 1242, Sept. 2003.
[13] A. K. Pandey and R. Pratap, "Effect of flexural modes on squeeze film damping in MEMS cantilever resonators," *J. Micromech. Microeng.*, vol. 17, no. 12, p. 2475, 2007.
[14] A. Duwel, J. Gorman, M. Weinstein, J. Borenstein, and P. Ward, "Experimental study of thermoelastic damping in MEMS gyros," *Sensor. Actuat. A-Phys.*, vol. 103, no. 1, pp. 70–75, 2003.
[15] S. Lepage, *Stochastic finite element method for the modeling of thermoelastic damping in micro-resonators*, PhD thesis, University of Liège, 2006.
[16] R. M. Patrikar, "Modeling and simulation of surface roughness," *Appl. Surf. Sci.*, vol. 228, no. 1, pp. 213–220, 2004.
[17] G. Palasantzas and J. T. M. De Hosson, "Pull-in characteristics of electromechanical switches in the presence of Casimir forces: Influence of self-affine surface roughness," *Phys. Rev. B*, vol. 72, no. 11, p. 115426, 2005.
[18] G. Palasantzas and J. T. M. DeHosson, "Surface roughness influence on the pull-in voltage of microswitches in presence of thermal and quantum vacuum fluctuations," *Surf. Sci.*, vol. 600, no. 7, pp. 1450–1455, 2006.
[19] W. Broer, G. Palasantzas, J. Knoester, and V. B. Svetovoy, "Significance of the Casimir force and surface roughness for actuation dynamics of MEMS," *Phys. Rev. B*, vol. 87, no. 12, p. 125413, 2013.
[20] D. S. Chandrasekharaiah and L. Debnath, *Continuum Mechanics*, Academic Press, 1994.
[21] H. Parkus, *Thermoelasticity*, Blaisdell Publishing Company, New York, 1968.
[22] M. Jaswon and G. Symm, *Integral Equation Methods in Potential Theory and Elastostatics*, Academic Press, New York, 1977.
[23] F. Shi, P. Ramesh, and S. Mukherjee, "On the application of 2D potential theory to electrostatic simulation," *Commun. Numer. Meth. En.*, vol. 11, no. 8, pp. 691–701, 1995.
[24] A. Alwan and N. Aluru, "Analysis of hybrid electrothermomechanical microactuators with integrated electrothermal and electrostatic actuation," *J. Microelectromech. Syst.*, vol. 18,

pp. 1126 –1136, Oct. 2009.
[25] A. Burgdorfer, "The influence of the molecular mean free path on the performance of hydrodynamic gas lubricated bearings," *Trans. ASME, Ser. D*, vol. 81, pp. 94–100, 1959.
[26] N. A. Cressie, *Statistics for Spatial Data, revised edition*, vol. 928, Wiley, New York, 1993.
[27] C. K. Williams and C. E. Rasmussen, *Gaussian processes for machine learning*, MIT Press, 2006.
[28] P. D. Sampson and P. Guttorp, "Nonparametric estimation of nonstationary spatial covariance structure," *J. Am. Stat. Assoc.*, vol. 87, no. 417, pp. 108–119, 1992.
[29] A. Alwan and N. Aluru, "A nonstationary covariance function model for spatial uncertainties in electrostatically actuated microsystems," *Int. J. Uncertain. Quantif.*, vol. 5, no. 2, pp. 99–121, 2015.
[30] A. Patil, D. Huard, and C. J. Fonnesbeck, "PyMC: Bayesian stochastic modelling in Python," *J. Stat. Softw.*, vol. 35, no. 4, p. 1, 2010.
[31] M. K. Poutous, Z. Hosseinimakarem, and E. G. Johnson, "Photoresist surface roughness characterization in additive lithography processes for fabrication of phase-only optical vortices," *J. Micro. Nanolithogr. MEMS MOEMS*, vol. 11, no. 4, pp. 043009–043009, 2012.
[32] O. Perrin and W. Meiring, "Identifiability for non-stationary spatial structure," *J. Appl. Probab.*, vol. 36, no. 4, pp. 1244–1250, 1999.